Detection and Identification of Multipath Interference With Adaption of Transmission Band for UWB Transceiver Systems

Sven Ole Schmidt, Horst Hellbrück

Technische Hochschule Lübeck - University of Applied Sciences, Germany
Department of Electrical Engineering and Computer Science

Abstract

In modern industrial wireless applications, communication between sensor nodes is indispensable. In the last years, ultra-wideband or UWB systems evolved for both data transfer and localization. Due to multipath propagation, a received RF signal is often a superposition of multiple echoes of the transmit signal, reflected on walls and other obstacles. The limited bandwidth of the transmit signal leads to constructive or destructive interference between the single signal echoes. An analysis of multipath propagation is challenging since interference is hard to detect, even for UWB signals. Therefore, we develop an interference model for adaptive UWB transmission bands and simulate the effects of interference. For reliable detection of multipath interference, we suggest adapting the transmission bands to vary the result of the interference. By applying the *Search Subtract and Readjust*-Algorithm of Falsi et al. in 2006, we achieve a reliable identification of signal echoes with improved resolution accuracy depending on the transmission bandwidth. For real systems with limited bandwidth, we assemble received signals of multiple distinct adjacent transmission bands, e.g., the UWB channels, to increase the bandwidth and thereby the resolution accuracy. We evaluate our approach by measurements and found that the resolution for correct identification of interfering signal echoes is improved from $2.32\,\text{ns}$ to $0.78\,\text{ns}$ by assembling signals from three transmission bands.

Keywords

Multipath Interference, Detection, Identification, Transmission Band, Ultra-Wideband, UWB Transceiver System, Signal Echo, Signal Assemblage

1. Introduction

The Internet of Things (IoT) is one of the most important application areas for localization. In the IoT, stationary and mobile devices exchange information wirelessly. The current position of devices adds the necessary context for interpreting the information provided by the devices, e.g. data of sensors in industrial production. State-of-the-art solutions employ a localization infrastructure with ultra-wideband (UWB) technology and multiple anchors to estimate the position of a tag by measurement of the signal propagation time (e.g. Time Distance of Arrival [1], Time of Flight [2]). Such systems with many anchors are costly in hardware and deployment as well as maintenance. To decrease the costs, a reduction of anchor hardware is beneficial. In recent publications, virtual anchors provide an approach for reducing the number of anchors

CEUR Workshop Proceedings (CEUR-WS.org)

[3]. These systems process and interpret multipath signals for an improved localization in a known environment. The work here is in this context of virtual anchor localization.

In wireless communication, a transmitted signal overlaps with echoes that occur in reflection paths and superpose at the receiver. In UWB technology embedded for localization, the received signal is processed with a time resolution in the range of nanoseconds to measure the arrival time of the pulses.

The multipath propagation and the resulting superposition of the signal echoes, e.g. at walls, deteriorate the performance of a localization system. If two interfering signal echoes are too close to each other, the superposition of these echoes prevents the identification of the origin signal echoes. The result of the interference changes for distinct transmission bands. To the best of our knowledge we are the first to investigate and exploit the usage of distinct transmission bands in real systems. By adapting the transmission band e.g. changing the UWB channel in the same radio environment and setup, the superposition of the signal echoes is detectable. By assembling the signals from distinct transmission bands we increase the reliability and resolution of identification of multipath interference.

The contributions of this paper are as follows:

- We design an UWB transceiver model including multipath signal propagation.
- We investigate the impact of transmission bands on interfering signal echoes and introduce a concept for detection of interference with an adaption of distinct transmission bands.
- We extend the *Search Subtract and Readjust*-Algorithm of [4] for identification of an arbitrary number of interfering signal echoes of UWB signals.
- We determine the minimum distance between two signal echoes for correct identification and show that the assemblage of multiple distinct received signals of several UWB channels increases the resolution.
- We evaluate the approach by real measurements.

The rest of the paper is organized as follows. Section 2 outlines related work in the field of UWB transceiver models, including multipath propagation and detection and identification of interference, as well as localization systems. In Section 3, we depict our proposed transceiver model and describe the impact of the transmission band on signal echo interference. Section 4 introduces our concept of interference detection and identification. Section 5 provides an evaluation of the approach with real measurements. Section 6 concludes the article and gives a short outlook on future work.

2. Related Work

In this section, we briefly summarize the current state-of-the-art of interference detection and identification.

Our concept of detection and identification is applied to modeled multipath propagation. In [5], Liberti et al. derived a general geometry-based model for multipath propagation, including a Line-of-Sight connection. Cimdins et al. addressed an UWB transceiver model with multipath in [6], but neglected interference by focusing on an interference-free setup. In this work, we

derive the UWB-channel model, including Friis-Path losses and the behavior of interfering signal echoes.

Multiple algorithms for estimation of the signal echo propagation delays are explored. In [7], Vanderveen et al. presented an ESPRIT-based approach for delay estimation of multipath transmitted signal echoes. Zhao et al. as well as Paredes et al., both developed an UWB channel estimator based on compressed sensing [8, 9]. Yang et al. introduced in [10] the CLEAN-algorithm for multipath channel estimation, which is based on the deconvolution technique. In contrast, we focus on the matched-filter theory for identification of the echoes. Yousef et al. formulate an algorithm for detection and identification of constructive signal echo interference following a RAKE-receiver approach [11]. However, in our work, we additionally covered destructive interference based on opposed signal echo phase states.

While some current localization systems mitigate the multipath interference, like Xie et al. [12] or Dogru et al. [13], our work focuses on identification of interference to exploit the corresponding information for further processing. Meanwhile, many localization systems rely on multipath propagation of UWB signals for position estimation. Systems like the device-free system MAMPI by Cimdins et al. [14] and the single anchor system SALMA by Großwindhager et al. [3] exploit this information. Also, Mohammadmoradi et al. developed an UWB single-anchor indoor localization system based on parameter distribution of the multipath propagation [15]. For this purpose, in our previous work [16], we developed a concept for positioning of the anchors of multipath-assisted localization systems, but we neglect the interference.

The proposed algorithm decreases the minimum needed resolution accuracy between two interfering signals, which is also important for other applications than UWB localization. The search for correct transmit signals to decline the influence of interference is also possible by the algorithm. Multiple image restoration systems suffer from interfering signals. Sharped images are recovered from blurred ones by application of deconvolution and matched filter approaches, similar to the proposed algorithm [17]. Also in medical ultra-sonic systems, pulse detection techniques are applied to reduce range sidelobe artifacts of pulse compression methods for more than 20 years [18].

3. Multipath Interference in UWB Transmissions

In this section, we introduce our UWB transceiver model, including multipath interference. Afterwards, we show how varying the transmission band affects the interference of signal echoes.

### 3.1. UWB Multipath Propagation and Interference of Signal Echoes

In this section, we analyze the impact of multipath propagation on received UWB signals $y(t)$. To generate the UWB transmit signal $x(t)$, we select a *center frequency* f_c and a *bandwidth B* to construct a rectangular transmission spectrum $X(f)$ of width B around f_c. In the following, this spectral range is called *transmission band* $\mathbf{B}_T = [f_c - B/2, f_c + B/2]$.

In time domain, the rectangular spectrum corresponds to a sinc-function, while the frequency shift by f_c transforms to a cosine-wave. So, $x(t)$ results to be a cosine-wave of frequency f_c,

which is weighted with a sinc-function with zeros in the range of $T = 1/B$ around $t = 0$:

$$x(t) = \sqrt{P_{Tx}} \cdot \frac{\sin(\pi \cdot t/T)}{\pi \cdot t/T} \cdot \cos(2\pi \cdot f_c \cdot t), \tag{1}$$

where $\sqrt{P_{Tx}}$ is the amplitude resulting from the given transmit power P_{Tx}. We have chosen this basic transmit signal representation to focus on the generality of the following theoretical derivation.
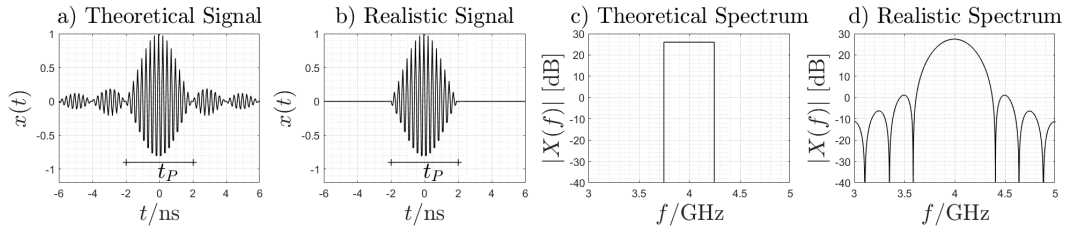
Figure 1: Transmit Signal $x(t)$ of UWB channel 2 at $\mathbf{B}_{T,2}$

Figure 1 shows the theoretical and the realistic UWB transmit signal $x(t)$ of UWB channel 2 on transmission band $\mathbf{B}_{T,2} = [3.75, 4.25]$ GHz as well as the corresponding spectrums $X(f)$. The main pulse width t_P results from the sinc-function in $x(t)$ and therefore from the chosen bandwidth with $t_P = 2/B = 4$ ns. Since the infinite sinc-function is not practicable in real transceiver systems, the transmission signal is cut to the main pulse of width t_P, like done e.g., for the Decawave DW1000-RF Chip [19]. This changes the transmission spectrum to a little broader spectrum. In the following, we will focus on the realistic transmit signal $x(t)$.

This signal $x(t)$ propagates from transmitter Tx to receiver Rx as illustrated in Figure 2. We assume that Tx omits $x(t)$ omni-directional into the free space with an ideal antenna. We also assume that the receiver Rx is not able to detect the angle of arrival of the incoming signal echoes.
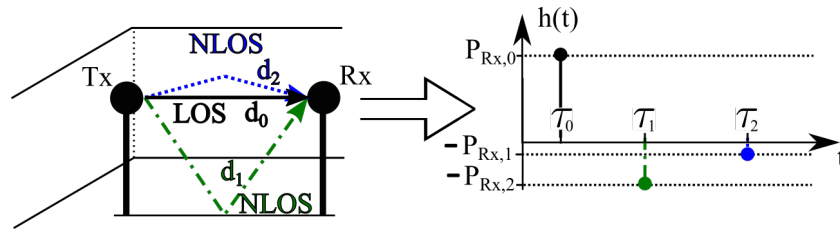
Figure 2: Multipath propagation including LOS and NLOS paths

The signal $x(t)$ transmitted on the *Line-Of-Sight*-Path (LOS) between Tx and Rx is always the first signal sensed by Rx. Additionally, $x(t)$ is reflected at obstacles like furniture or walls and reaches Rx as well. The signal echoes traveling the *Non-Line-Of-Sight*-Paths (NLOS) result in a longer distance, e.g. d_i for the i-th path. The I signals $x(t)$ reaching Rx are called *signal*

echoes. We assume an ideal transmission and disregard noise and interference by other devices in this work.

Each signal echo is received after a specific propagation delay $\tau_i = d_i/c_0$ (speed of light $c_0 \approx 3 \cdot 10^8$ m/s) with a characteristic receive power $P_{Rx,i}$ for the i-th path, $i = 0, ..., I - 1$. The power $P_{Rx,i}$ results from the given transmit power P_{Tx}, decreased by the distance-depending *Friis Free Space Path-Losses* $P_{PL,i}$ with path-loss coefficient γ:

$$P_{Rx,i} = \frac{P_{Tx}}{P_{PL,i}}, \text{ with} \tag{2}$$

$$P_{PL,i} = \left(\frac{4\pi \cdot d_i \cdot f_c}{c_0} \right)^{\gamma} = (4\pi \cdot \tau_i \cdot f_c)^{\gamma}, \tag{3}$$

Each reflection at a surface of a material with a higher refractive index than the transmission medium causes an additional phase shift of π (inverting the signal). By definition, in NLOS paths, the signal echoes $x(t)$ are reflected at least once, with $n_i \geqslant 1$.

All single signal echoes superpose at the receiver Rx. They differ in propagation delay, power level and phase shift. The *Channel Impulse Response* (CIR) $h(t)$ describes the overall multipath propagation with I paths:

$$
\begin{aligned}
h(t) &= \sum_{i=0}^{I-1} (-1)^{n_i} \sqrt{\frac{1}{P_{PL,i}}} \cdot \delta(t - \tau_i) \\
&= f_c^{-\frac{\gamma}{2}} \sum_{i=0}^{I-1} (-1)^{n_i} (4\pi \cdot \tau_i)^{-\frac{\gamma}{2}} \cdot \delta(t - \tau_i),
\end{aligned}
\tag{4}
$$

where $\delta(t - \tau_i)$ is the Dirac-Function shifted by τ_i. Eq. (4) shows that the CIR of distinct transmission bands differs only in scaling factor depending on center frequency f_c. The CIR of the setup shown on the left of Figure 2 is sketched on the right. With increasing delay τ_i, the receive power $R_{Rx,i}$ decreases.

The received signal $y(t)$ is the convolution of the CIR $h(t)$ with the signal $x(t)$:

$$
\begin{aligned}
y(t) &= x(t) * h(t) \\
&= f_c^{-\frac{\gamma}{2}} \sum_{i=0}^{I-1} (-1)^{n_i} (4\pi \cdot \tau_i)^{-\frac{\gamma}{2}} \cdot x(t - \tau_i).
\end{aligned}
\tag{5}
$$

Figure 3 shows a received signal $y(t)$ on transmission band $\mathbf{B}_{T,2}$ including three signal echoes. Here, the signal on the LOS path with delay $\tau_0 = 1.66$ ns is received without any interference. The echoes with delay $\tau_1 = 6.8$ ns and $\tau_2 = 8.13$ ns interfere, because the delay difference $\Delta\tau = |\tau_2 - \tau_1| = 1.33$ ns is smaller than the main pulse width $t_P = 4$ ns > 1.33 ns. While the single signal echoes are marked in green and blue, the period of interference is marked in red color. The result of the interference of two signal echoes is modeled in the next step.
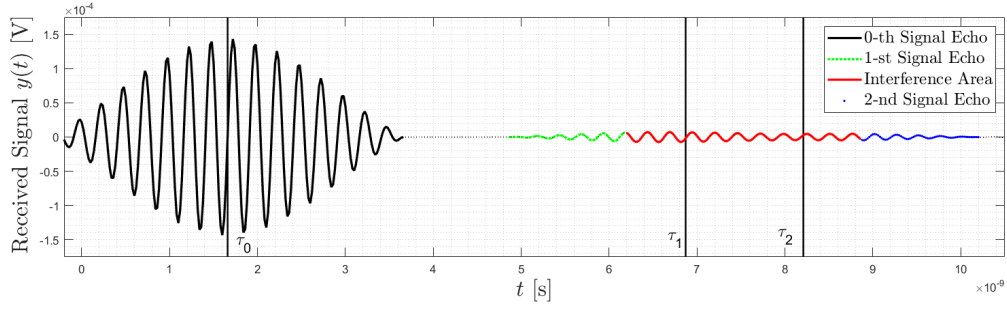
Figure 3: Exemplary received signal $y(t)$ with three signal echoes

3.2. Impact of the Transmission Band on Signal Echo Interference

This subsection investigates the impact of transmission bands on the interference of two signal echoes. As shown in Figure 1, we assume a main pulse width $t_p = 2/B$ for the given realistic signal $x(t)$. Therefore, two signal echoes with delay τ_i and τ_j do interfere, if the delay difference $\Delta\tau = |\tau_i - \tau_j| < t_p = 2/B$. According to Eq. (1), the oscillation of signal $x(t)$ corresponds to the center frequency f_c of $\mathbf{B}_T$. Therefore, $x(t)$ of duration t_P includes $t_P \cdot f_c$ oscillations of periodic time $T_0 = 1/f_c$.

The oscillation phase at time t_0 is named phase state $\Theta(t_0)$ and depends on f_c as the period of the oscillation is $1/f_c$. The phase difference between two signal echos i and j is constant:

$$\Delta\Theta_{i,j} = |\Theta_j - \Theta_i| = 2\pi \cdot |\tau_j - \tau_i| \cdot f_c = 2\pi \cdot \Delta\tau \cdot f_c \qquad (6)$$
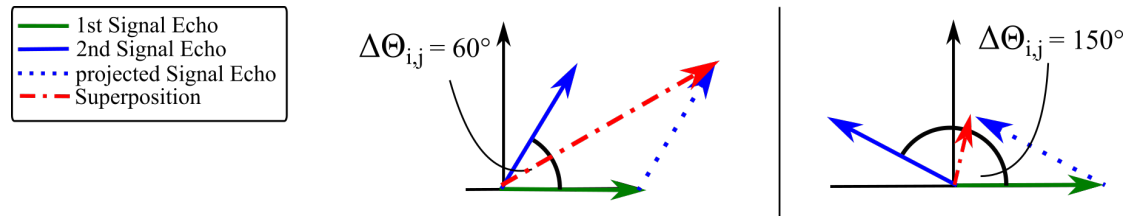
**Figure 4:** Superposition of two signal echoes depending on $\Delta\Theta_{i,j}$

This phase difference $\Delta\Theta_{i,j}$ is important for a constructive or destructive superposition. Figure 4 depicts two results for $\Delta\Theta_{i,j} = \{60°, 150°\}$. On the left, the superposition of the samples results in an overall stronger magnitude (constructive interference). When $\Delta\Theta_{i,j}$ is increased by $90°$, as depicted in the right plot, the sum results in mitigation of the superposed magnitude (destructive interference). It is important to note that the phase shift in these two cases may result from only a change of the center frequency. To illustrate the effect of the change of the center frequency f_c of the transmission band $\mathbf{B}_T$ on the interference, the superposition

of two interfering signal echos i and j is shown, with $\tau_i = 6.87\,\text{ns}$, $\tau_j = 8.2\,\text{ns}$ and $\Theta_i(t_0) = 0°$. This delay difference of $\Delta\tau = 1.33\,\text{ns}$ results in completely different phase shifts $\Delta\Theta_{i,j}$ for the three selected UWB channels 1, 2 and 3 as shown in Table 1 and Figure 5.

Table 1
Band $\mathbf{B}_{T,k}$ of UWB channels $1, 2, 3$ as well as resulting phase difference $\Delta\Theta_{1,2}(\Delta\tau = 1.33\,\text{ns})$.

UWB channel k	$\mathbf{B}_{T,k}$ [GHz]	$f_{c,k}$ [GHz]	$\Delta\Theta_{i,j}(1.33\,\text{ns})$
1	$[3.25, 3.75]$	3.5	$240°$
2	$[3.75, 4.25]$	4.0	$120°$
3	$[4.25, 4.75]$	4.5	$0°$
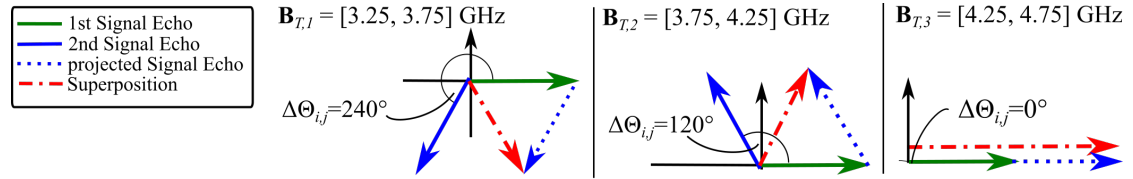
Figure 5: Impact of UWB channel $\mathbf{B}_{T,k}$ on the signal echo superposition

The transmission bands of the UWB channels 1 and 2 superpose to the same magnitude as the phase difference $\Delta\Theta_{i,j}$ is $\pm120°$. Choosing the transmission band $\mathbf{B}_{T,3}$ of UWB channel 3 leads to the phase difference $\Delta\Theta_{i,j} = 0°$, which corresponds to the maximum constructive superposition. Since $\Delta\Theta_{i,j}$ is constant (independent of time) for the signal echoes i and j, the superposition is also constant (either destructive or constructive) for the total period of interference.

Note, that the phase difference $\Delta\Theta_{i,j}$ is always equal for two transmission bands, if $f_{c,1} = l \cdot f_{c,2}$ holds, with $l \in \mathbb{N}$. The impact of the transmission band on the superposition of signal echoes is applied in the next section to detect and identify interference.

4. Detection and Identification of Interference with transmission band analysis

In this section, we first introduce our approach for detection and identification of interfering signal echoes and calculate the resolution and limitations. Second, we show how to improve the resolution accuracy by combining multiple transmission bands.

4.1. Detection of Interference by Adaption of Transmission Bands

In the last section, we depicted, how the transmission band $\mathbf{B}_T$ affects the superposition of two interfering signal echoes. Since the overall magnitude of the superposition varies, depending on the chosen center frequency f_c, the adaption of f_c evinces interference in the received signal $y(t)$. Neglecting the scalar factor $f_c^{-\gamma/2}$ (comp. to Eq. (5)), the complex envelope's magnitude $|y_c(t)|$

of the received signal $y(t)$ of multiple distinct transmission bands only differs in the period of interfering signal echoes. To calculate $y_c(t)$, we shift the received signal from the transmission band at center frequency f_c back to baseband at $f_c^0 = 0\,\mathrm{Hz}$ and apply a lowpass-filter.
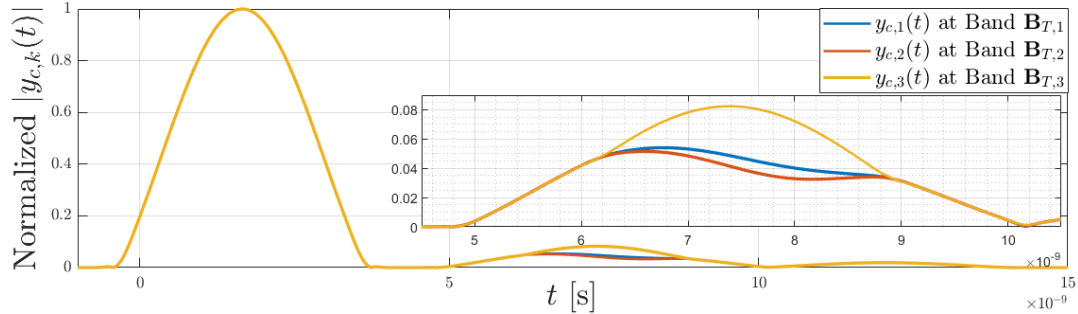
Figure 6: Detection of Interference by Comparison

Figure 6 shows the magnitude of the complex envelopes $y_{c,1}(t), y_{c,2}(t)$ and $y_{c,3}(t)$, for a certain multipath setup with $\tau_0 = 1.66\,\mathrm{ns}$, $\tau_1 = 6.87\,\mathrm{ns}$, $\tau_2 = 8.2\,\mathrm{ns}$ and $\tau_3 = 12.05\,\mathrm{ns}$. The chosen transmission bands are the UWB channels 1, 2 and 3 of Table 1. Due to the bandwidth of $B = 500\,\mathrm{MHz}$, the echoes at delay τ_1 and τ_2 interfere with delay difference of $\Delta\tau = 1.33\,\mathrm{ns}$, which corresponds to the setup in Figure 5.

As expected, the non-interfering signal echoes at τ_0 and τ_3 do not differ for the distinct transmission bands. However, the magnitude of the highlighted period of interference changes with the frequency. While the complex envelope's magnitudes of the transmission bands $\mathbf{B}_{T,1}$ and $\mathbf{B}_{T,2}$ are nearly equal, the envelope's magnitude of transmission band $\mathbf{B}_{T,3}$ is maximal at this area.

4.2. Identification of Signal Echoes with the *Search Subtract and Readjust*-Algorithm

For identification of an unknown number of signal echoes in the received signal, we modified the *Search Subtract and Readjust*-algorithm (**SSR**) of Falsi et al. [4]. The SSR was originally designed to identify a known number of delays of overlapping LOS connections of multiple transmitters Tx in multipath-suffering UWB received signals. In our setup, we do not know the number of signal echoes in advance. Algorithm 1 depicts, how the individual propagation delays $\hat{\tau}$ and amplitudes $\hat{\mathbf{a}}$ are estimated by the modified SSR-algorithm until a threshold is reached.

First, a received signal $y_{It}(t)$, the amplitude threshold a_t, and counter c are initialized. Next, the iterative algorithm starts and proceeds as long as none of the estimated amplitudes is smaller than the threshold, with $|\hat{\mathbf{a}}[c']| \geqslant a_t$ (Line 1-9).

Neglecting noise and following Eq. (5), the overall received signal $y(t)$ is equivalent to the CIR $h(t)$ which was convolved (filtered) with the transmit signal $x(t)$. We apply the matched filter approach to find the corresponding propagation delays and amplitudes of the signal echoes

---
Algorithm 1: Modified Pseudo code for Search Subtract and Readjust Algorithm from [4]

Data:
received signal $y_{It}(t) = y(t)$;
threshold: $a_t \in \mathbb{R}^+$;
counter: $c \leftarrow 1$;

1   **while** $\nexists \, c'\!: |\hat{\mathbf{a}}[c']| < a_t$ **do**

2     $y_{conv}(t) = y_{It}(t) * x(-t)$;

3     $\hat{\tau}[c] \leftarrow \underset{t \in \mathbb{R}^+}{\arg \max}(y_{conv}(t))$;

4     $w_c(t) = x(t - \hat{\tau}[c])$;

5     $\mathbf{w}_{cmb} = \left[w_1[kT_S]^T, ..., w_c[kT_S]^T \right]^T, \, k \in \mathbb{N}$;

6     $\begin{bmatrix} \hat{\mathbf{a}}[1] \\ \vdots \\ \hat{\mathbf{a}}[c] \end{bmatrix} = \left[\mathbf{w}_{cmb} \cdot \mathbf{w}_{cmb}^T \right]^{-1} \times \left[\mathbf{w}_{cmb} \cdot y[kT_S]^T \right]$;

7     $c = c + 1$;

8     $y_{It}(t) = y(t) - \sum_{i=1}^{c} \hat{\mathbf{a}}[i] \cdot x(t - \hat{\tau}[i])$;

9   **end**

---

in $y(t)$. In Line 2 we convolve our processed received signal $y_{It}(t)$ with $x(-t)$, the conjugate time-reversed version of $x(t)$, and determine the argument $\hat{\tau}[c]$, which maximizes the resulting $y_{conv}(t)$ (Line 3).

Next, we calculate the estimated amplitudes $\hat{\mathbf{a}}$ of all delays $[\hat{\tau}(1), ..., \hat{\tau}(c)]$. For this, we define $w_c(t)$ as signal $x(t)$ shifted by $\hat{\tau}[c]$ (Line 4) and discretize it with sample time T_S to align it with the predefined shifted signals in matrix $\mathbf{w}_{cmb}$ in Line 5, $k \in \mathbb{N}$. In Line 6 we multiply the original received signal $y(t)$ with $\left(\left[\mathbf{w}_{cmb} \cdot \mathbf{w}_{cmb}^T \right]^{-1} \times \mathbf{w}_{cmb} \right)$, the pseudo-inverse of $\mathbf{w}_{cmb}$, to (re-)estimate all amplitudes $\hat{\mathbf{a}}$.

Afterward, we increase the counter c by one and determine the new $y_{It}(t)$ as the difference between $y(t)$ and the estimated signal echoes with respective propagation delay and amplitude.

We predict that the resolution accuracy for identification of interfering signal echoes is limited to a minimum delay difference $\Delta\tau$. Signal echoes with smaller $\Delta\tau$ are not distinguished and may not be identified anymore.

4.3. Assemblage of Signals of distinct Transmission Bands

The predefined resolution accuracy depends on the pulse width $t_P = 2/B$ and, therefore, on bandwidth B of transmission band $\mathbf{B}_T$. A way to decrease t_P and increase the resolution accuracy is to increase the bandwidth B. As for real systems, the bandwidth is limited. So, we suggest adjusting the transmission band and performing several measurements combined in further signal processing.

We combine the measured received signals $y_k(t)$ of transmission bands $\mathbf{B}_{T,1}$, $\mathbf{B}_{T,2}$ and $\mathbf{B}_{T,3}$ (see Table 1). Adding up the spectrum of these signals assembles a transmission band

$\mathbf{B}_{T,a} = [3.25, 4.75]$ GHz with bandwidth $B = 1.5$ GHz. This is possible, if the corresponding combined transmit signal $x_a(t)$ is similar to the transmit signal $x_h(t)$ of the homogeneous transmission band $\mathbf{B}_{T,h} = [3.25, 4.75]$ GHz.
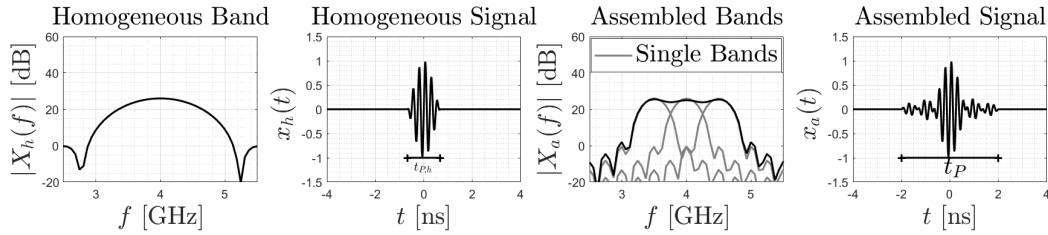
Figure 7: Assembled transmit signal $x_a(t)$ compared to homogeneous signal $x_h(t)$

Figure 7 depicts the transmission bands $\mathbf{B}_{T,a}$ and $\mathbf{B}_{T,h}$, as well as the corresponding transmit signals $x_a(t)$ and $x_h(t)$. Note, that for $x_h(t)$, we consider the realistic pulse shape with $t_{P,h} = 3 \cdot 2/B = 1.33$ ns. The cross-correlation of both variants of signal results in $\mathbf{xcorr}(x_a(t), x_h(t)) = 96.7\%$. For the main pulse width $t_{P,h}$, the similarity is 99.8%. Thus applied:

$$x_h(t) \approx x_a(t) = \sum_{k=1}^{3} x_k(t) \tag{7}$$

Note, that the pulse width of $x_a(t)$ is still $t_{P,a} = t_P = 4$ ns. Following Eq. (5), also the corresponding received signal $y_a(t)$ of the signal $x_a(t)$ is the sum of all received signals with:

$$y_a(t) = x_a(t) * h(t)$$
$$= \sum_{k=1}^{3} x_k(t) * h(t) = \sum_{k=1}^{3} y_k(t). \tag{8}$$

In summary, the assembled transmit signals are very similar to the homogeneous signal. We will investigate how much the assemblage increases the resolution accuracy of signal echo identification compared to single transmission bands.

4.4. Increasing Accuracy for Identification of Signal Echoes

The modified SSR-algorithm, introduced in Section 4.2, identifies an unknown number of interfering signal echoes. We assume that the reconstruction is possible up to a certain resolution in the form of a delay difference $\Delta\tau$ of the echoes. In this section, we analyze simulated received signals $y_1(t), y_2(t)$ and $y_3(t)$ of transmission bands $\mathbf{B}_{T,1}, \mathbf{B}_{T,2}$ and $\mathbf{B}_{T,3}$ for this resolution. Additionally, we generate the assembled $y_a(t)$ with Eq. (8). We suppose, that reducing the main pulse width $t_{P,h} < t_P$ and increasing the bandwidth will improve the resolution.

As input, a multipath propagation with two signal echoes is set up accordingly. The first signal echo has a delay $\tau_1 = 14$ ns and for the second one, we choose a flexible delay of $\tau_2 =$

$[10, 14]$ ns with a spacing of 0.01 ns between the single values, resulting in a delay difference of $\Delta\tau = [4, 0]$ ns. Both echo paths include $n_1 = n_2 = 1$ reflection and the path loss coefficient is $\gamma = 2$. For modeling these received signals, we follow Eq. (1) and Eq. (5).

Since the algorithm stops when at least one estimated amplitude is smaller than the pre-defined threshold a_t, first the number of estimated signal echoes N_{SE} is of interest. Based on the known receive power $P_{Rx,i}$, we choose $a_t = 0.08$.
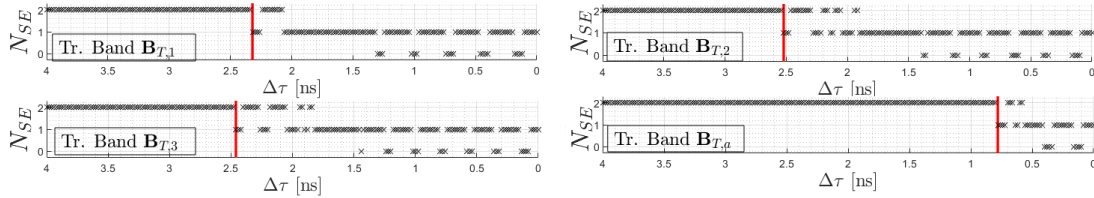
Figure 8: Number of SSR-estimated signal echoes N_{SE}

Figure 8 shows the N_{SE} for the received signals $y_1(t)$, $y_2(t)$, $y_3(t)$ and $y_a(t)$ for a decreasing delay difference of $\Delta\tau = [4, 0]$ ns between two signal echoes.

Table 2 lists the delay difference for the first erroneous and the last correct number of estimated signal echoes N_{SE}, as well as the overall percentage of wrong estimations for all four transmission bands. The first erroneous estimation for N_{SE} is also marked in the single plots.

Table 2
Delay difference of the first erroneous and last correct calculation of N_{SE}, as well as the relative number of erroneous estimations.

Bands	first error ($\Delta\tau$)	last correct ($\Delta\tau$)	$\frac{\text{Errors}}{\text{All Setups}}$
$\mathbf{B}_{T,1}$	2.32 ns $= 0.58 \cdot t_P$	2.08 ns $= 0.52 \cdot t_P$	59.5%
$\mathbf{B}_{T,2}$	2.52 ns $= 0.63 \cdot t_P$	1.92 ns $= 0.48 \cdot t_P$	54.5%
$\mathbf{B}_{T,3}$	2.46 ns $= 0.62 \cdot t_P$	1.84 ns $= 0.46 \cdot t_P$	53.0%
$\mathbf{B}_{T,a}$	0.78 ns $= 0.20 \cdot t_P$	0.58 ns $= 0.15 \cdot t_P$	17.5%

The single transmission bands $\mathbf{B}_{T,1}$, $\mathbf{B}_{T,2}$ and $\mathbf{B}_{T,3}$ result in similar delay differences for the first occurring erroneous as well as for and the last correct estimated number of signal echoes. The relative number of erroneous estimates moves in the same range.

As expected due to increase of the bandwidth, these results are decreased by the assemblage to the combined received signal $y_a(t)$. While the first occurring error is at least 1.54 ns $= 0.38 \cdot t_P$ smaller, the last correct estimation for N_{SE} is decreased by at least 1.26 ns $= 0.31 \cdot t_P$. Also, the relative number of errors is decreased by a minimum 35.5%.

The difference between the estimation for the delays of the signal echoes $\hat{\tau}[1]$ and $\hat{\tau}[2]$ and the origin delays τ_1 and τ_2 is calculated by the ℓ_1-norm:

$$d_e(\Delta\tau) = \sum_{i=1}^{2} |\tau_i - \hat{\tau}[i]| \tag{9}$$
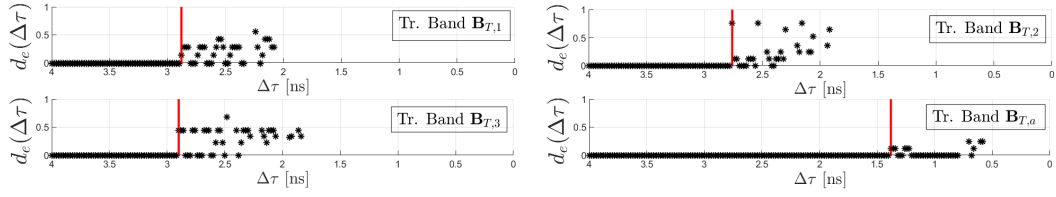
Figure 9: ℓ_1-norm $d_e(\Delta\tau)$ for all SSR results with $N_{SE} = 2$

Figure 9 depicts the estimation errors $d_e(\Delta\tau) > 0$ of all SSR-results with $N_{SE} = 2$ for the transmission bands $\mathbf{B}_{T,1}$, $\mathbf{B}_{T,2}$, $\mathbf{B}_{T,3}$ and $\mathbf{B}_{T,a}$.

Table 3 lists the delay difference for the first error and the overall percentage of wrong estimations in all estimations for all four transmission bands. The first occurring erroneous estimation $d_e(\Delta\tau) > 0$ is also marked in the single plots.

Table 3
Delay Difference of the first erroneous delay estimation with $d_e(\Delta\tau) > 0$ as well as the relative number of erroneous estimations.

Bands	first error with $d_e(\Delta\tau) > 0$	$\frac{\text{Erroneous Delay}}{\text{All correct} N_{SE}}$
$\mathbf{B}_{T,1}$	$\Delta\tau = 2.88$ ns $= 0.72 \cdot t_P$	28%
$\mathbf{B}_{T,2}$	$\Delta\tau = 2.76$ ns $= 0.69 \cdot t_P$	24%
$\mathbf{B}_{T,3}$	$\Delta\tau = 2.90$ ns $= 0.73 \cdot t_P$	32%
$\mathbf{B}_{T,a}$	$\Delta\tau = 1.38$ ns $= 0.35 \cdot t_P$	6%

Again, the three single transmission bands result in similar values for the first occurring erroneous delay estimation. Also, the relative number of errors with respect to the successful estimation of the numbers of signal echoes with $N_{SE} = 2$ does not vary much either. This proves the existence of the *resolution accuracy*. It limits the minimum needed delay difference $\Delta\tau$ for correct identification of N_{SE}, as well as for the correct estimation of delays $\hat{\tau}[1]$ and $\hat{\tau}[2]$.

Applying the SSR on the assembled $y_a(t)$ of the three transmission bands lowers the delay difference $\Delta\tau$ of the first occurring erroneous delay estimation by at least 1.38 ns $= 0.35 \cdot t_P$. The relative number of erroneous delay estimations is also decreased. Note that the resulting overall number of 10 erroneous delay estimations is also the lowest overall number for all four considered transmission bands. So, the assembling of the single distinct transmission bands decreases the minimum needed $\Delta\tau$ and increases the resolution accuracy of the SSR.

In the next section, we evaluate the approach and algorithms by real measurements.

5. Evaluation

In this section, we depict our measurement setup and evaluate our approach for detection and identification of interference additionally by real measurements. Also, we investigate if the combination of transmission bands works the same as the homogeneous spectrum.

5.1. Measurement Setup

The measurement setup is designed in relation to Figure 2. It is installed in an indoor environment with transmitter Tx and receiver Rx at the height of $0.84\,\mathrm{m}$ with a distance of $d_0 = 0.3\,\mathrm{m}$ and omnidirectional PCB antennas. The predicted delay is $\tau_0 \approx 1\,\mathrm{ns}$. Another signal echo passes a ground reflection with a path length of $d_1 = 1.7\,\mathrm{m}$ and a delay of $\tau_1 = 5.7\,\mathrm{ns}$.

Additionally, a static but flexible reflector is placed at a distance of $1.04\,\mathrm{m}$ to the LOS, resulting in a path length of $d_2 = 2.1\,\mathrm{m}$ and delay of $\tau_2 = 7\,\mathrm{ns}$. The difference between the reflector path length and the ground path results in a delay difference of $\Delta\tau = 1.33\,\mathrm{ns}$.

A last signal component is a reflection at the ceiling with a path length of $d_3 = 3.8\,\mathrm{m}$ and delay $\tau_3 = 12.7\,\mathrm{ns}$. This signal echo neither interferes with the ground signal echo nor with the reflector signal echo.

For measurement, we transmit three signals $x_k(t)$ $(k = 1, 2, 3)$ in three different transmission bands $\mathbf{B}_{T,1}$, $\mathbf{B}_{T,2}$ and $\mathbf{B}_{T,3}$ (see Table 1) with a Tektronix AWG 70002A arbitrary waveform generator with transmit power $P_{Tx} = 180\,\mathrm{mW}$. The received signals $y_1(t)$, $y_2(t)$ and $y_3(t)$ are measured by a Tektronix DPO 72304DX oscilloscope. We calculate the mean of 5.000 measurements for each received signal to decrease the environmental noise.

For the determination of the transmission delays of these signal echoes an usual 8th generation Intel Core i7 processor needs around $0.25\,\mathrm{s}$. Since this unit works separately to the UWB signal exchange, both setups are parallelizable. So, also the usage of common UWB hardware is possible, if the transmit pulse and the signal alternation due to the hardware are known.

5.2. Detection of measured Interference by Adaption of Transmission Bands
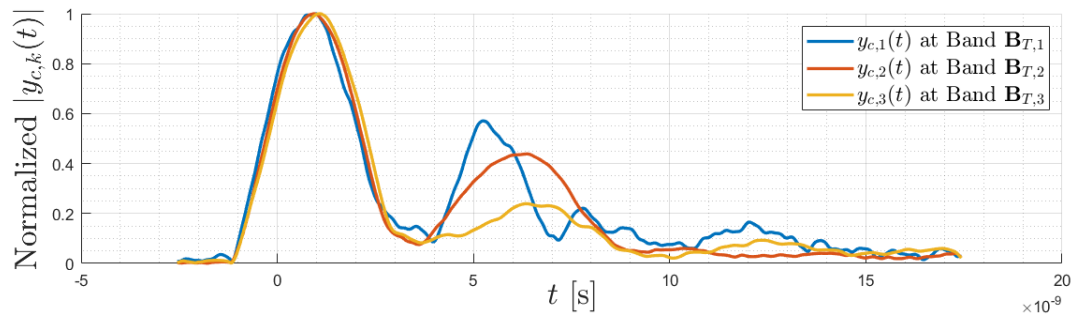
Figure 10: Detection of measured Interference

Figure 10 depicts the complex envelopes of the measured received signals of the UWB Channels 1, 2 and 3 (at $\mathbf{B}_{T,1}$, $\mathbf{B}_{T,2}$ and $\mathbf{B}_{T,3}$). We see a large variation of the amplitude of the received signals $y_{c,1}(t)$, $y_{c,2}(t)$ and $y_{c,3}(t)$ in the expected period of interference. Between $[3.75, 9]\,\mathrm{ns}$ interfering signal echoes from ground and reflector path vary similar to the simulation results in Figure 6. There are additional signal echoes around $13\,\mathrm{ns}$ resulting from longer signal paths in our indoor environment. The measurements confirm our findings from Section 4.1 when we adopt the transmission band and compare the resulting complex envelopes of the magnitude.

5.3. Assemblage of measured Received Signals of distinct Transmission Bands

Next, we will analyze if assembling distinct received signals increases the bandwidth of the transmission band to evaluate if the resolution of the multipath detection increases the same way as a comparable homogeneous spectrum. Therefore, we create the signal $x_h(t) = x_a(t)$ from Figure 7 and measure the received signal $y_h(t)$ with a total bandwidth of 1.5 GHz. As expected from Section 4.3, the shape of both received signals $y_h(t)$ and $y_a(t)$ are very similar with a cross correlation coefficient of $\mathbf{xcorr}(y_a(t), y_h(t)) = 98.79\%$. It proves that assembling received signals of distinct transmission bands provides the same benefits as a homogeneous signal with the same bandwidth.

5.4. Identification of Interference of Measured Received Signals

Finally, we will investigate the performance of the modified SSR-algorithm introduced in Section 4.2 with the measured received signals. For this, we choose an amplitude threshold of $a_t = 0.1 \cdot |y_{c,k}(\tau_0)|$. This is a good approximation for the expected amplitude relation $\sqrt{P_{Rx,0}/P_{Rx,2}} \approx 0.14$ (see Eq. (2)) for the highest covered center frequency $f_{c,3} = 4.5$ GHz, with path-loss coefficient $\gamma = 2$.

Table 4
SSR-based delay estimation of measured interfering echoes at $\tau_1 = 5.7$ ns and $\tau_2 = 7$ ns for band $\mathbf{B}_{T,k}$

Band	N_{SE}	$\hat{\tau}[1]$	$\hat{\tau}[2]$	$d_e(\Delta\tau)$
$\mathbf{B}_{T,1}$	2	5.6 ns	7.64 ns	0.74 ns
$\mathbf{B}_{T,2}$	2	6 ns	7.66 ns	0.96 ns
$\mathbf{B}_{T,3}$	1	6.62 ns	—	—
$\mathbf{B}_{T,a}$	2	5.74 ns	7.04 ns	0.08 ns

Table 4 illustrates the results for all signals. For the signals $y_1(t)$ and $y_2(t)$ the algorithm detects the correct number of signal echoes N_{SE} for the measured setup, and achieves an accuracy of 0.74 ns and 0.96 ns respectively. The SSR-algorithm does not provide the correct number of signal echoes for signal $y_3(t)$. Based on the interference, the algorithm has estimated the wrong delay $\hat{\tau}[1]$ with too high $\hat{\mathbf{a}}[1]$. This caused the amplitude of the estimated delay $\hat{\tau}[2]$ to fall below the threshold $\hat{\mathbf{a}}[2] < a_t$. When assembling these received signals to $y_a(t)$, the reliability and the accuracy is increased to $d_e(\Delta\tau) = 0.08$ ns, which corresponds to an averaged delay identification error of approximately 0.04 ns $= 1.25$ cm for each of the two signal echoes.

As derived in Section 4.2, the limited bandwidth of 500 MHz results in unreliable and imprecise identification of the signal echoes with distance $\Delta\tau = 1.3$ ns. By assembling three signals into $y_a(t)$ and increasing the bandwidth to 1.5 GHz, the identification performs precisely and reliably.

6. Conclusion and Future Work

In this paper, we introduced a concept for detection and identification of multipath interference based on an adaption of the transmission bands for UWB signals. We showed by a systematic

analysis that switching the transmission band, namely the center frequency, changes the phase difference between interfering signal echoes and, therefore, the interference, namely the amplitude of the resulting signal. By this, varying amplitude interference of signal echoes is detectable in a multipath setup in theory and measured in practical experiments. With the assemblage of the signals from multiple distinct transmission bands, we can even identify several signal echoes with an accuracy of $d_e(\Delta\tau) = 0.08\,\text{ns}$, which corresponds to a distance error of approximately 2.5 cm. As the concepts are implemented and confirmed by real measurements, our solution for detection and identification of interference is ready for application in real localization systems.

In the future, we will implement an application with out-of-box hardware like the DecaWave DW1000-RF-Chip and extend the algorithms to adjust for a dynamic multipath environment. Subsequently, we will embed the detection and identification approach in a real localization system. In this context we will focus on the increase of localization accuracy by application of the proposed algorithm compared to other approaches. Also we will evaluate the trade-off between accuracy and the computional complexity and the influence of external interfering devices in the future.

Acknowledgements

References

[1] S. Leugner, H. Hellbrück, Lessons learned: Indoor Ultra-Wideband localization systems for an industrial IoT application, Technical Report, Technische Universität Braunschweig, 2018. doi:`10.24355/dbbs.084-201807191244-0`.

[2] J. Wang, Q. Gao, Y. Yu, X. Zhang, X. Feng, Time and energy efficient tof-based device-free wireless localization, IEEE Transactions on Industrial Informatics 12 (2016) 158–168. doi:`10.1109/TII.2015.2501225`.

[3] B. Großwindhager, M. Rath, J. Kulmer, M. S. Bakr, C. A. Boano, K. Witrisal, K. Römer, Salma: Uwb-based single-anchor localization system using multipath assistance, in: Proceedings of the 16th ACM Conference on Embedded Networked Sensor Systems, SenSys '18, Association for Computing Machinery, New York, USA, 2018. doi:`10.1145/3274783.3274844`.

[4] C. Falsi, D. Dardari, L. Mucchi, M. Z. Win, Time of arrival estimation for UWB localizers in realistic environments, EURASIP Journal on Advances in Signal Processing 2006 (2006). doi:`10.1155/asp/2006/32082`.

[5] J. Liberti, T. Rappaport, A geometrically based model for line-of-sight multipath radio channels, in: Proceedings of Vehicular Technology Conference - VTC, volume 2, 1996, pp. 844–848 vol.2. doi:`10.1109/VETEC.1996.501430`.

[6] M. Cimdins, S. O. Schmidt, H. Hellbrück, Modeling the magnitude and phase of multipath uwb signals for the use in passive localization, in: 2019 16th Workshop on Positioning, Navigation and Communications (WPNC), 2019, pp. 1–6. doi:10.1109/WPNC47567.2019.8970256.

[7] M. Vanderveen, A.-J. Van der Veen, A. Paulraj, Estimation of multipath parameters in wireless communications, IEEE Transactions on Signal Processing 46 (1998) 682–690. doi:10.1109/78.661335.

[8] Zhao, Lili, Zhang, Peng, Dong, Qicai, Huang, Xiangyang, Zhao, Jianhua, Su, Zeyu, Research of the channel estimation in wireless communication systems, ITM Web Conf. 25 (2019). doi:10.1051/itmconf/20192501002.

[9] J. L. Paredes, G. R. Arce, Z. Wang, Ultra-wideband compressed sensing: Channel estimation, IEEE Journal of Selected Topics in Signal Processing 1 (2007) 383–395. doi:10.1109/JSTSP.2007.906657.

[10] W. Yang, Z. Naitong, Z. Qinyu, Z. Zhongzhao, Deconvolution techniques for characterizing indoor uwb wireless channel, Journal of Systems Engineering and Electronics 19 (2008) 688–693. doi:10.1016/S1004-4132(08)60140-1.

[11] N. Yousef, A. Sayed, Detection of fading overlapping multipath components for mobile positioning systems, in: ICC 2001. IEEE International Conference on Communications. Conference Record (Cat. No.01CH37240), volume 10, 2001, pp. 3102–3106 vol.10. doi:10.1109/ICC.2001.937243.

[12] T. Xie, C. Zhang, Y. Li, H. Jiang, Z. Wang, An enhanced tdoa approach handling multipath interference in wi-fi based indoor localization systems, in: 2017 IEEE 60th International Midwest Symposium on Circuits and Systems (MWSCAS), 2017, pp. 160–163. doi:10.1109/MWSCAS.2017.8052885.

[13] S. Dogru, L. Marques, Through-wall mapping using radar: Approaches to handle multi-path reflections, IEEE Sensors Journal 21 (2021) 11674–11683. doi:10.1109/JSEN.2021.3067721.

[14] M. Cimdins, S. O. Schmidt, H. Hellbrück, Mampi-uwb—multipath-assisted device-free localization with magnitude and phase information with uwb transceivers, Sensors 20 (2020). doi:10.3390/s20247090.

[15] H. Mohammadmoradi, M. Heydariaan, O. Gnawali, K. Kim, Uwb-based single-anchor indoor localization using reflected multipath components, in: 2019 International Conference on Computing, Networking and Communications (ICNC), 2019, pp. 308–312. doi:10.1109/ICCNC.2019.8685609.

[16] S. O. Schmidt, M. Cimdins, H. Hellbrück, On the effective length of channel impulse responses in uwb single anchor localization, in: 2019 International Conference on Localization and GNSS (ICL-GNSS), 2019. doi:10.1109/ICL-GNSS.2019.8752644.

[17] A. Levin, Y. Weiss, F. Durand, W. T. Freeman, Understanding and evaluating blind deconvolution algorithms, in: 2009 IEEE Conference on Computer Vision and Pattern Recognition, 2009, pp. 1964–1971. doi:10.1109/CVPR.2009.5206815.

[18] B. Haider, P. Lewin, K. Thomenius, Pulse elongation and deconvolution filtering for medical ultrasonic imaging, IEEE Transactions on Ultrasonics, Ferroelectrics, and Frequency Control 45 (1998) 98–113. doi:10.1109/58.646915.

[19] DW1000 Datasheet, Decawave Ltd 2015, 2015. Version 2.09.